A Machine Learning approach to distinguish between regular and chaotic motions of space debris in the geopotential approximation

Alessandra Celletti (UNITOV), Giuseppe Pucacco (UNITOV),
Christos Efthymiopoulos (Padova), Victor Rodriguez (UPM),
Catalin Gales (UAIC)

Stardust-R, Local Training Workshop I, Madrid, Spain, May 18–21 2020

May 20, 2020

STARDUST

PUSHING THE BOUNDARIES OF
SPACE RESEARCH TO SAVE OUR FUTURE

Abstract and objectives

This activity has the aim to investigate the dynamics of a specific region of the sky around the Earth, in order to distinguish between regular and chaotic motions. The steps that allow to reach this goal are the following:

- We start from a model problem which describes the motion of a forced pendulum. The model will be given using Hamiltonian formalism and the corresponding Hamilton's equations.

- We integrate the equations of motion and compute its Poincaré map to understand the difference between rotational, librational, chaotic motions;

- We consider the dataset corresponding to a particle orbiting around the Earth; like in the pendulum, the dataset describes rotational, librational, chaotic motions for different values of the elements (mean anomaly and semimajor axis). An index is assigned to distinguish between rotational, librational, chaotic motion;

- We implement a Machine Learning algorithm to get information for a large number of initial conditions and assign the binary index to each initial condition.

Space debris dynamics

PHYSICS

◇ Conservative regime in MEO, GEO Regions affected by the monopole term of the Earth's attraction, Earth's oblateness J_2 and J_{22}, attraction of the Moon, influence of the Sun and SRP.

◇ Dissipative regime in LEO. Region affected also by the atmospheric drag.

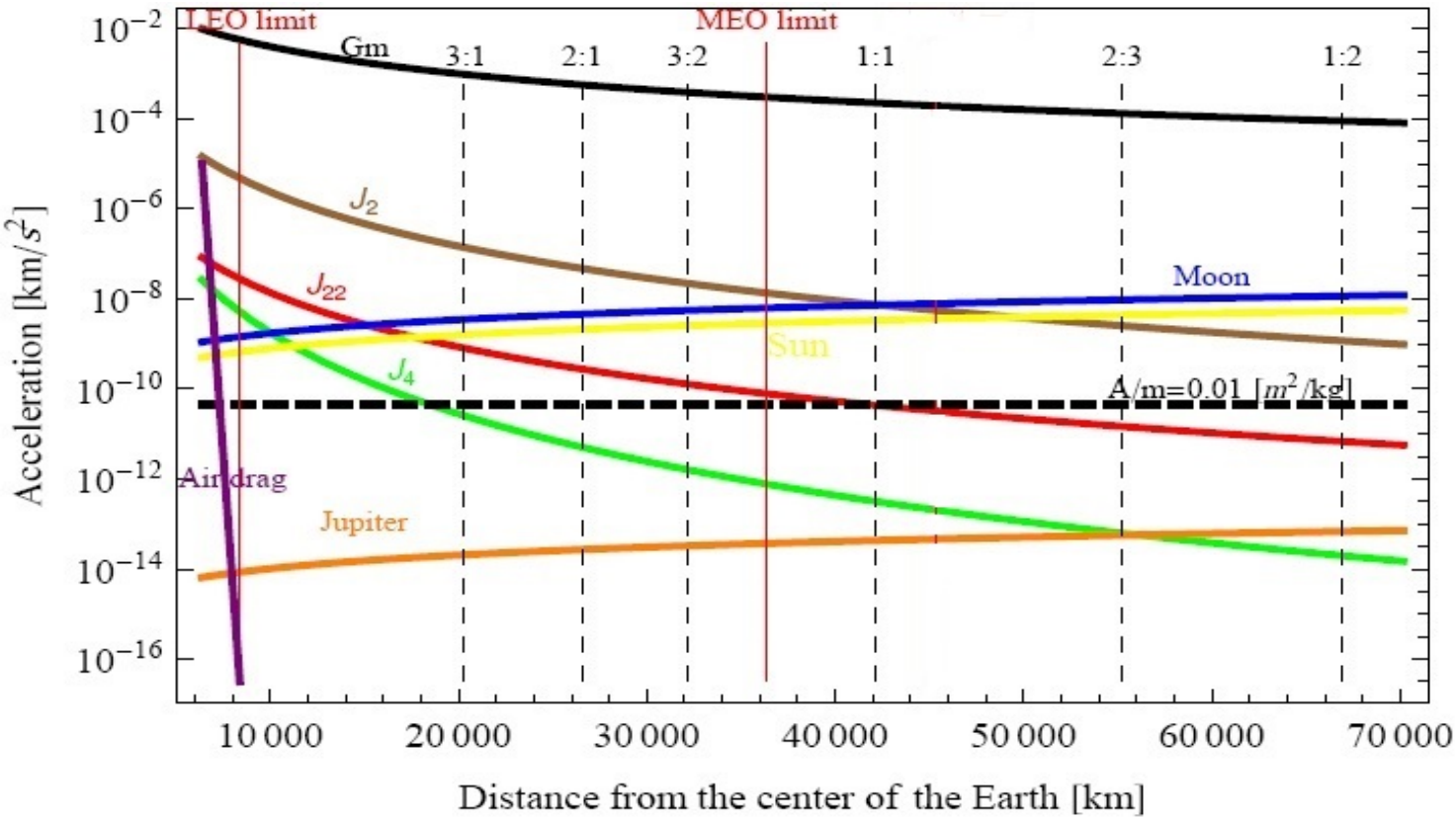

Figure : Order of magnitude of various perturbations of a satellite orbit.

• DYNAMICS

The long-term evolution of satellite orbits depends on various effects:

◇ **A) Gravitational resonances**

–**Tesseral resonances** occur whenever there is a commensurability between the orbital period of a satellite and the period of Earth's rotation. Main effect: a variation of the semi-major axis on time scales of the order of hundred of days (see Breiter (2005), Valk et al. (2009), Celletti et al. (2014, 2015))

–**Lunisolar resonances** involve commensurabilities between slow angles: ω, Ω, ω_M, Ω_M, M_S. Main effect: variations of eccentricity and inclination on time scales of the order to tens (or hundred) of years. (see Rosengren et al. (2015), Daquin et al. (2016), Alessi et al. (2016), Celletti et al. (2016, 2017), Gkolias et al. (2019).

◇ **B) Solar radiation pressure** influences the orbits of high area-to-mass ratio objects (HAMR). Main effects: periodic motion of the orbital elements; in particular annual periodic motion of the eccentricity (see Valk et al. (2008, 2009)). **Secondary resonances** involving and the Sun's longitude (see Lemaître et al. (2009)).

◇ **C) Dissipation.** Different atmospheric models give different results (see Petit and Lemaitre (2017)); Combined effect of air drag and resonances (tesseral or lunisolar) have been addressed recently (Celletti and CG (2018), Alessi et al. (2018)).

◇ **D)** Various **dynamical phenomena** like overlapping of resonances (tesseral or secular) and the onset of chaos (see Celletti et al. (2014–2017), Rosengren et al. (2015), Daquin et al. (2016)), bifurcations of equilibria Celletti et al. (2016,2017), interplay between conservative and dissipative effects (Celletti and CG (2018)), etc.

Canonical equations

• The action–angle Delaunay variables $(L, G, H, M, \omega, \Omega)$ are related to the orbital elements $(a, e, i, M, \omega, \Omega)$ by

$$L = \sqrt{\mu_E a}\,, \qquad G = L\sqrt{1-e^2}\,, \qquad H = G\cos i\,.$$

The dynamical equations of motion are given by

$$\dot{M} = \frac{\partial \mathcal{H}}{\partial L}\,, \qquad \dot{\omega} = \frac{\partial \mathcal{H}}{\partial G}\,, \qquad \dot{\Omega} = \frac{\partial \mathcal{H}}{\partial H}$$
$$\dot{L} = -\frac{\partial \mathcal{H}}{\partial M}\,, \qquad \dot{G} = -\frac{\partial \mathcal{H}}{\partial \omega}\,, \qquad \dot{H} = -\frac{\partial \mathcal{H}}{\partial \Omega}\,,$$

the Hamiltonian is given by

$$\mathcal{H} = -\frac{\mu_E^2}{2L^2} + \mathcal{H}_{Earth}(a, e, i, M, \omega, \Omega, \theta) + \mathcal{H}_{Moon}(a, e, i, M, \omega, \Omega, \Lambda_M)$$
$$+\mathcal{H}_{Sun}(a, e, i, M, \omega, \Omega, \Lambda_S) + \mathcal{H}_{SRP}(a, e, i, M, \omega, \Omega, \Lambda_S)\,.$$

with $\mu_E = \mathcal{G}\, m_E$, θ sidereal time, Λ_M, Λ_S = orbital elements of Moon w.r.t. ecliptic and Sun w.r.t. celestial equator.

Tesseral resonances

• The Fourier expansion of $\mathcal{H}_{Earth}$ has the form (Kaula 1966, Chao 2005):

$$\mathcal{H}_{Earth} = \frac{\mu_E}{a} \sum_{n=2}^{\infty} \sum_{m=0}^{n} \left(\frac{R_E}{a}\right)^n J_{nm} \sum_{p=0}^{n} F_{nmp}(i) \sum_{q=-\infty}^{\infty} G_{npq}(e)\, cs_{nm}\Big(\Psi_{nmpq}(M,\omega,\Omega,\theta)\Big)$$

where R_E is the radius of the Earth, J_{nm} are the harmonic coefficients, F_{nmp}, G_{npq} are the inclination and eccentricity functions, cs_{nm} is the cosine (sine) function if $n-m$ is even (odd) and

$$\Psi_{nmpq}(M,\omega,\Omega,\theta) = (n-2p)\omega + (n-2p+q)M + m(\Omega-\theta) - m\lambda_{nm}\ .$$

•*Tesseral/gravitational resonances*, whenever the period of debris and the rotation of the Earth are commensurable, i.e. $\ell\dot{M} - j\dot{\theta} \simeq 0$, $\ell, j \in \mathbb{N}$, is satisfied.
• We focus on the 1:1 and 2:1 resonances, that is $\dot{M} - \dot{\theta} \simeq 0$ and $\dot{M} - 2\dot{\theta} \simeq 0$, which occur at around 42164 km and respectively at 26560 km from the center of the Earth.

The Fast Lyapunov Indicator (FLI). Description of the data

• For each resonance, we average $\mathcal{H}_{Earth}$ over fast angles and obtain:

$$\mathcal{H}_{Earth} \cong \mathcal{H}^{sec}_{Earth} + \mathcal{H}^{res\, j:\ell}_{Earth},$$

where $\mathcal{H}^{sec}_{Earth}$ and $\mathcal{H}^{res\, j:\ell}_{Earth}$ are the secular and resonant parts. Topologically, the dynamics of the resonant Hamiltonian is similar to a forced pendulum.

• We integrated numerically the canonical equations, referred hereafter by

$$\frac{d\mathfrak{X}}{dt} = \mathcal{F}(\mathfrak{X}, t),$$

and the the variational equations associated

$$\frac{dV}{dt} = \frac{\partial \mathcal{F}}{\partial \mathfrak{X}}(\mathfrak{X}, t)V.$$

• Given an initial condition $\mathfrak{X}(0)$, the Maximum Lyapunov Exponent (MLE) and the fast Lyapunov indicator (hereafter FLI) are defined by (C. Froeschlé et al. 1997)

$$MLE(\mathfrak{X}(0)) \equiv \lim_{t\to\infty} \frac{1}{t} \log \frac{||V(t)||}{||V(0)||}, \qquad FLI(\mathfrak{X}(0), V(0), T) \equiv \sup_{0<t\leq T} \log \frac{||V(t)||}{||V(0)||}.$$

We computed FLI up to a time $T = 19$ years.

• We compute a grid of 100x100 points of the $\sigma - a$ plane, where for the 1:1 resonance the critical angle is $\sigma = \lambda = M - \theta + \omega + \Omega$, while for the 2:1 resonance $\sigma = M - 2\theta + \omega + 2\Omega$.

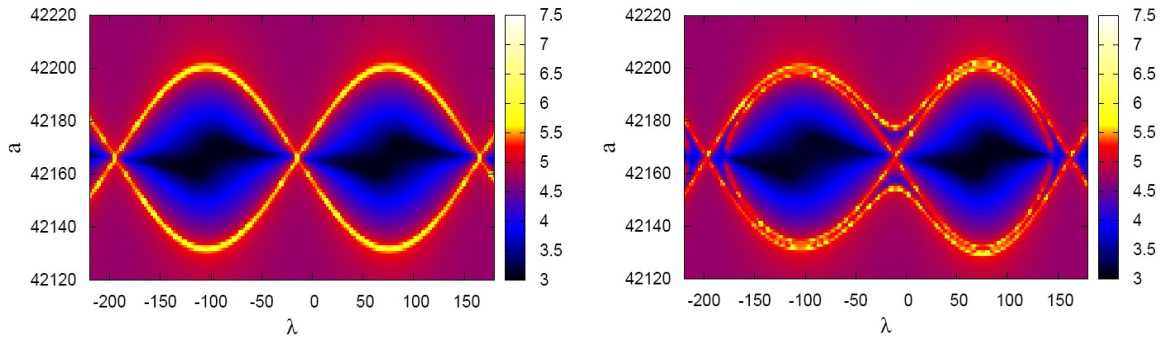

Figure : FLI for the GEO 1:1 resonance for $e = 0.005$, $i = 0^o$, $\omega = 0$, $\Omega = 0$, under the effects of the J_2 and J_{22} terms (left); all harmonics up to degree and order $n = m = 3$ (right). (Reproduced from Celletti and Gales (2014), see the top plots of Figure 3.)

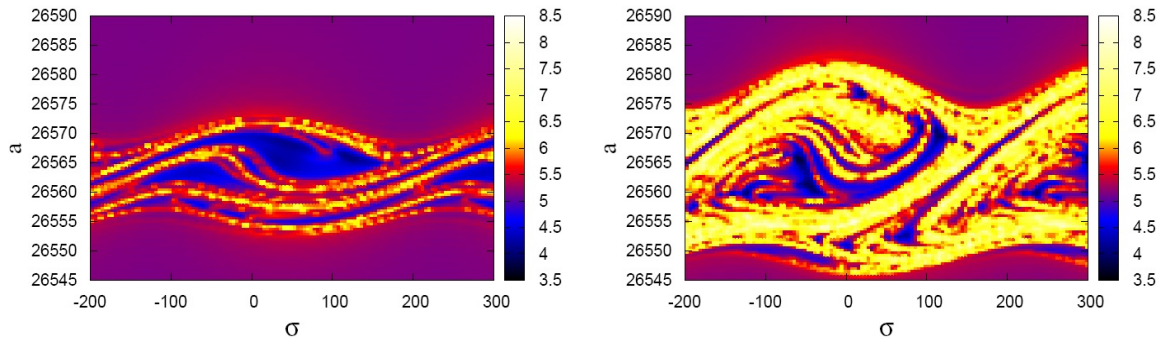

Figure : FLI for the MEO 2:1 resonance, under the effects of all harmonics up to degree and order $n = m = 4$, for $i = 30^o$, $\omega = 0$, $\Omega = 0$: $e = 0.1$ (left); $e = 0.5$ (right). (Reproduced from Celletti and Gales (2014), see the bottom plots of Figure 9.)

• The files *left_fig*3_*index*012.*plt*, *right_fig*3_*index*012.*plt* are linked to the 1:1 resonance, and *left_fig*9_*index*012.*plt*, *right_fig*9_*index*012.*plt* are obtained for the 2:1 resonance.

• The (nine) columns of these four files provide the following data:1) the resonant angle σ (in degrees); 2) the semi-major axis a (in km); 3)-8) the value of FLI after 1 year, 2, 3, 5, 10 and 19 years, respectively; 9) a (dynamical) index with the following meaning: 0–chaotic motion, 1–regular non–resonant (rotational) motion, 2–regular resonant (librational) motion;

```
-220.0000 42120.0000 3.4150441 3.7837017 3.9355429 4.1532148 4.4703858 4.7593767 1.0
-216.0000 42120.0000 3.4206633 3.7781785 3.9201391 4.1687252 4.4572785 4.7467398 1.0
-212.0000 42120.0000 3.4264156 3.7681471 3.9066486 4.1666446 4.4461705 4.7361155 1.0
-208.0000 42120.0000 3.4317922 3.7559496 3.8951312 4.1567644 4.4371142 4.7425995 1.0
-204.0000 42120.0000 3.4365347 3.7451543 3.8856405 4.1488712 4.4465170 4.7384181 1.0
-200.0000 42120.0000 3.4405943 3.7363710 3.8782092 4.1430860 4.4553503 4.7341196 1.0
-196.0000 42120.0000 3.4440788 3.7296280 3.8728664 4.1394287 4.4558828 4.7319665 1.0
-192.0000 42120.0000 3.4471985 3.7249459 3.8696348 4.1379192 4.4555502 4.7319751 1.0
-188.0000 42120.0000 3.4502171 3.7223428 3.8685221 4.1385574 4.4572308 4.7341425 1.0
-184.0000 42120.0000 3.4534128 3.7218203 3.8695315 4.1413399 4.4591460 4.7384584 1.0
-180.0000 42120.0000 3.4570509 3.7233836 3.8726567 4.1462612 4.4547937 4.7449043 1.0
-176.0000 42120.0000 3.4613654 3.7270178 3.8778807 4.1532891 4.4414137 4.7359802 1.0
-172.0000 42120.0000 3.4665496 3.7327067 3.8851817 4.1623912 4.4514879 4.7465614 1.0
-168.0000 42120.0000 3.4727511 3.7404044 3.8945058 4.1735097 4.4635729 4.7591406 1.0
-164.0000 42120.0000 3.4800708 3.7500626 3.9057919 4.1865750 4.4775818 4.7692278 1.0
-160.0000 42120.0000 3.4885630 3.7615947 3.9189498 4.1953735 4.4934112 4.7716469 1.0
-156.0000 42120.0000 3.4982361 3.7748860 3.9338483 4.1891671 4.5100864 4.7895917 1.0
-152.0000 42120.0000 3.5090528 3.7897800 3.9503287 4.1681522 4.4928024 4.7898841 1.0
-148.0000 42120.0000 3.5209295 3.8060706 3.9681663 4.1791727 4.5130058 4.8105390 1.0
-144.0000 42120.0000 3.5337360 3.8234866 3.9870821 4.1993219 4.5341821 4.8120912 1.0
-140.0000 42120.0000 3.5472930 3.8416892 4.0067214 4.2201392 4.5559731 4.8342680 1.0
-136.0000 42120.0000 3.5613697 3.8602427 4.0266469 4.2411786 4.5567811 4.8532605 1.0
```

Figure : Data description.

Remarks

• The values of FLI at $T = 19$ years (8th column) are used to make a cartography the phase space of the 1:1 and 2:1 resonances as in the above Figures reproduced from Celletti and Gales (2014) (top plots of Figure 3 for the GEO 1:1 resonance, and respectively bottom plots of Figure 9 for the MEO 2:1 resonance), where darker colors denote a regular dynamics (either rotational or librational motions), while lighter colors denote chaotic behavior. The values of FLI at $T = 19$ years (8th column) are also used to assign the (dynamical) index of the 9th column.
• Machine learning algorithm are used in connection with the values of FLI provided in the columns 3)–6).
• Since the values of FLI in the columns 3)-6) are obtained after integrating the equations for a very short interval of time, this approach could be a very fast and powerful tool to investigate various topics in the space debris dynamics.
• Machine learning algorithm could be a very efficient tool to make a preliminary study of disposal orbits, which are influenced by secular resonances.

References

• A. Celletti, C. G., *On the dynamics of space debris: 1:1 and 2:1 resonances*, J. Nonlinear Science 2014.